Targeted Intraceptor Nanoparticle Therapy Reduces Angiogenesis and Fibrosis in Primate & Murine Macular Degeneration

Ling Luo[1,2], **Xiaohui Zhang**[1], **Yoshio Hirano**[3], **Puneet Tyagi**[4], **Péter Barabás**[1], **Hironori Uehara**[1], **Tadashi R. Miya**[1], **Nirbhai Singh**[1], **Bonnie Archer**[1], **Yureeda Qazi**[1], **Kyle Jackman**[1], **Subrata K. Das**[1], **Thomas Olsen**[1], **Srinivas R. Chennamaneni**[1], **Brian C. Stagg**[1], **Faisal Ahmed**[1], **Lyska Emerson**[5], **Kristen Zygmunt**[6], **Ross Whitaker**[6], **Christina Mamalis**[1], **Wei Huang**[1], **Guangping Gao**[7], **Sangly P. Srinivas**[8], **David Krizaj**[1], **Judit Baffi**[3], **Jayakrishna Ambati**[3], **Uday B. Kompella**[4], and **Balamurali K. Ambati**[1,*]

[1]Moran Eye Center, University of Utah, Salt Lake City,UT,USA, 84132

[2]Department of Ophthalmology, the 306th Hospital of PLA, Beijing, China, 10010

[3]University of Kentucky, Lexington, KY, USA, 40536

[4]University of Colorado-Denver, Skaggs School of Pharmacy, Aurora, CO, USA, 80262

[5]University of Utah, Dept. of Pathology, Salt Lake City, UT, USA, 84132

[6]University of Utah, Scientific Computing and Imaging Institute, Salt Lake City, UT, USA, 84132

[7]University of Massachusetts, Worcester, MA, USA, 01605

[8]Indiana University, Bloomington, IN, USA, 47405

Abstract

Monthly intraocular injections are widely used to deliver protein-based drugs that cannot cross the blood-retina barrier for the treatment of leading blinding diseases such as age-related macular degeneration (AMD). This invasive treatment carries significant risks, including bleeding, pain, infection, and retinal detachment. Further, current therapies are associated with a rate of retinal fibrosis and geographic atrophy significantly higher than that which occurs in the described natural history of AMD. A novel therapeutic strategy which improves outcomes in a less invasive manner, reduces risk, and provides long-term inhibition of angiogenesis and fibrosis is a felt medical need. Here we show that a single intravenous injection of targeted, biodegradable nanoparticles delivering a recombinant *Flt23k* intraceptor plasmid homes to neovascular lesions in the retina and regresses CNV in primate and murine AMD models. Moreover, this treatment suppressed subretinal fibrosis, which is currently not addressed by clinical therapies. Murine vision, as tested by OptoMotry©, significantly improved with nearly 40% restoration of visual loss induced by CNV. We found no evidence of ocular or systemic toxicity from nanoparticle treatment. These findings offer a nanoparticle-based platform for targeted, vitreous-sparing, extended-release, nonviral gene therapy.

Keywords

nanoparticles; gene delivery; choroidal neovascularization models; anti-VEGF therapy; angiogenesis

Leading retinal causes of blindness (*e.g.*, age-related macular degeneration (AMD),[1–4] angioid streaks, choroidal rupture, and high myopia) share the development of choroidal neovascularization (CNV) – the growth of fibrovascular tissue from the choriocapillaris into the subretinal space – as the underlying etiology of vision loss. Vascular endothelial growth factor (VEGF) plays a central role in CNV development.[5–9] Currently, the primary treatment for CNV consists of monthly injections of antibody-based inhibitors of VEGF into the vitreous.[9–11] Although this therapy improves visual acuity in a substantial proportion of patients, half of the eyes experience ongoing CNV leakage, fibrotic scarring and/or geographic atrophy.[12] Most patients do not experience substantial visual improvement, and a third of treated eyes continue to lose visual acuity and progress to legal blindness.[12] Frequent intravitreal injections represent a significant financial burden and entail risks that include bleeding, infection, traumatic injury, and retinal tear, detachment and degeneration.[9,13] A novel therapeutic strategy which improves outcomes in a less invasive manner, thereby reducing risk, and providing long-term inhibition of angiogenesis in a lesion-targeted manner is a felt medical need.[14]

Among the potential VEGF inhibitory strategies, anti-VEGF expressing nanoparticles are a promising approach capable of targeting VEGF intracellularly.[14–17] Advantages of using nanoparticles for gene delivery include sustained delivery, avoidance of viral-induced inflammation, immunogenicity and toxicity, and ease of production.[14,15,17–21] Intracellular VEGF targeting has an advantage in the case of cells responding to their own VEGF secretion in an autocrine fashion, as internal autocrine signaling would not inhibited by an extracellular VEGF-neutralizing antibody.[22] Autocrine loops have been reported in endothelial cells.[23] The anti-VEGF intraceptor, Flt23K, is a recombinant construct of VEGF binding domain 2 and 3 of VEGFR-1 (vascular endothelial growth factor receptor-1, Flt-1) coupled with the endoplasmic reticulum (ER) retention signal sequence lysine-aspartic acid-glutamic acid-lucine (KDEL).[22,23] KDEL is a peptide retention signal that binds ER retention receptors and prevents secretion of endogenous ER proteins coupled to KDEL. Flt23K intraceptors bind VEGF intracellularly with high affinity and sequester it within the ER, inhibiting VEGF secretion and the VEGF autocrine loop, enhancing the effects of VEGF inhibition.[14,22,23]

CNV also involves subretinal fibrosis, which can adversely affect vision even if angiogenesis resolves. Unfortunately, current treatments for AMD do not address fibrosis. Therefore, combinations of anti-angiogenic and anti-fibrotic factors with long-term effects have been suggested to more effectively improve vision.[24] Integrins are the main mediators of the interaction between fibroblasts and extracellular matrix (ECM) during scar formation. The tripeptide adhesion motif Arg-Gly-Asp (RGD) is contained in the ECM and binds αvβ3 and α5β1 integrins, which are selectively expressed in areas of neovascularization and scarring.[14,20,25,26] Our previous studies have found that nanoparticles are generally uptaken by cells through phagocytosis and that peptide targeting facilitates uptake by specific cell types.[27,28] Therefore, intravenous delivery of RGD-coated nanoparticles could possibly target anti-VEGF therapy specifically to CNV and reduce fibrosis and angiogenesis while reducing the neural retinal toxicity (*e.g.*, geographic atrophy) associated within travitreal delivery of extracellular anti-VEGF agents.[12,29]

Laser-induced CNV models are widely used due to their ease of quantification, although laser injury differs from AMD due to the laser's acute injury and retinal burnout with no potential for recovery of visual function. We demonstrated that CNV could be induced by knockdown of sFlt-1 (a soluble isoform of VEGF receptor-1, which acts as a naturally occurring inhibitor of VEGF-A mediated angiogenesis) via subretinal injection of adeno-associated viral (AAV) delivery of a short hairpin RNA (shRNA) targeting sFLT-1 (AAV.shRNA.*sFlt-1*).[30] In this study, we further explore whether this model could be used to test visual recovery with inhibition of CNV progression.

We developed an intracellular anti-angiogenic therapy relying on a three component system:[14] 1) Plasmids expressing *Flt23k* intraceptors, which consists of the VEGF-binding domains 2–3 of *Flt* (the highest-affinity VEGF receptor); 2) PLGA biodegradable nanoparticles as a delivery system; 3) the tripeptide adhesion motif Arg-Gly-Asp (RGD) to coat nanoparticles and facilitate selective homing to CNV after systemic intravenous injection. We demonstrated that this three component system can inhibit laser-induced CNV in rats.[14] In this study, we further analyzed this targeted nanoparticle system and assessed whether it could regress neovascularization, decrease fibrotic scarring, improve visual acuity, and demonstrate safety profile in two murine CNV models and a primate CNV model.[21]

Results

Nanoparticle characterization

Characteristics of the nanoparticles are summarized in Table and Fig. S1. Plasmid loading in nanoparticles was 1.02 and 1.30% w/w for RGD.*Flt23k*.NR.NP and *Flt23k*.NR.NP, respectively. Mean particle sizes were 572, 523, and 530 nm for the RGD.*Flt23k*.NR.NP, *Flt23k*.NR.NP, and Blank.NR.NP nanoparticles, respectively. Zeta potentials were −22.67, −27.69 mV, and −2.11 mV for *Flt23k*.NR.NP, Blank.NR.NP, RGD conjugated nanoparticles (RGD.*Flt23k*.NR.NP), respectively. RGD peptide (which contains positively charged amino acids) neutralizes the negatively charged carboxyl groups in the polymer. The size of the RGD.Blank.NR.NP is 163.7 nm (± 13.3 nm). Polydispersity is 0.349 (±0.08). The zeta potential is - 0.591mV (± 0.04 mV).

We measured the polydispersity index (PDI) of the nanoparticles after preparation and found it to be ~0.100. A low PDI indicates that the particles are of uniform size, whereas a higher PDI hints at aggregation due to irregular size distribution. Therefore, we speculate that the nanoparticles are not aggregated during preparation and storage. However, the *in vivo* fate of nanoparticles is different. PLGA nanoparticles are rapidly internalized via clathrin-mediated endocytosis. Further, modified nanoparticles such as RGD.*Flt23k*.NP can escape early endosomes to reach the cytosol.[27, 31] As the PLGA polymer is susceptible to acid hydrolysis, endosomes (having a low pH of 5.0) can deplete the nanoparticles of their surface polyvinyl alcohol (PVA) and cause aggregation. Therefore, *in vivo* conditions can lead to aggregation. The release kinetics result (Fig. S2) indicates that the *Flt23k* plasmid is released from RGD.*Flt23k*.NP and*Flt23k*.NP until 42 days and 35 days.

AAV.shRNA.*sFlt-1*-induced murine CNV model

The CNV phenotype induced by subretinal delivery of AAV.shRNA.*sFlt-1* resembles cardinal features of neovascular AMD in humans with regard to its chronicity, progression, and morphology (Fig. 1). CNV lesions grew towards the retina, as is observed clinically.[30] Secondary CNV lesions occurred and were separated both in distance and time from primary CNV (Fig. 1A). Besides classic CNV, subretinal fluid and intrachoroidal CNV were detected (Fig. 1B). These neovascular lesions remained physiologically active even at 6

months post-injection, as indicated by positive isolectin staining (Fig. 1C). Therefore, these patterns of CNV progression closely resemble the pathological course of CNV seen clinically in neovascular AMD, and the visual acuity in these eyes could possibly be restored by reversal of architectural changes. However, in laser-induced CNV this restoration is not possible due to partial retina burnout (Fig. 1D).

We observed alpha5 integrin expression by immunohistochemical (IHC) staining which demonstrates that alpha5 integrin is expressed strongly in AAV.shRNA.*sFlt-1* induced CNV model, as well as in laser-CNV murine and primate models, suggesting RGD coated nanoparticles could possibly specifically target CNV through the alpha5 integrin recognition sequence RGD (Fig. 1E).

RGD-functionalized nanoparticles localize to CNV lesions

RGD-functionalized PLGA nanoparticles loaded with anti-angiogenic plasmid *Flt23k* and conjugated with Nile Red (RGD.*Flt23k*.NR.NP) were detected by the Heidelberg Spectralis® imager *in vivo* in CNV eyes and normal eyes (Fig. 2A). The nanoparticles were first visualized in retinal blood vessels approximately 30 seconds following intravenous injection, and thereafter leaked and diffused evenly throughout the retinal vasculature. The higher density of nanoparticles in the fundus was observed for approximately 30 minutes and then decreased over time and was minimal at 1 hour post-injection. More nanoparticles were observed in CNV eyes than in normal eyes (Fig. 2A). Upon histological confocal examination of ocular cryosections (Fig. 2B) obtained 24 hours post-intravenous administration of nanoparticles, the nanoparticles were found to be primarily localized to CNV lesions. Nanoparticles were also occasionally observed in normal areas in CNV eyes and normal eyes, primarily in the outer segment layer of the neural retina and retinal pigment epithelium (RPE), with minimal amounts elsewhere in the neural retina. In the murine CNV model, RGD-coated nanoparticles were detected in CNV lesions at 14 days post-injection while in normal eyes nanoparticles were only seen up to 7 days post-treatment (Fig. 2B). Consistent with this finding, in monkey CNV models the RGD-conjugated nanoparticles but not unconjugated or blank nanoparticles were detected in CNV lesions at 1 month post-injection (Fig. 2C), indicating that RGD modified nanoparticles persisted in CNV lesions for extended periods of time.

RGD nanoparticles regress CNV

In the laser-induced CNV monkey model, the average CNV (staining by Perlecan antibodies) volumes were $7.7\pm1.0\times10^6\mu m^3$ (n=14), $13.1\pm1.8\times10^6\mu m^3$ (n=16), $11.4\pm0.5\times10^6\mu m^3$ (n=8) and $20.0\pm5.3\times10^6\mu m^3$ (n=19), in RGD.*Flt23k*.NR.NP, *Flt23k*.NR.NP, Blank.NR.NP, and sham control respectively. The average fibrosis (staining by Collagen I antibodies) volumes were $0.8\pm0.2\times10^6\ \mu m^3$, $1.6\pm0.2\times10^6\ \mu m^3$, $1.9\pm0.2\times10^6\ \mu m^3$ and $1.9\pm0.2\times10^6\ \mu m^3$ in RGD.*Flt23k*.NR.NP, *Flt23k*.NR.NP, Blank.NR.NP, and sham control respectively. This means, the CNV volumes at 4 weeks after treatment with RGD.*Flt23k*.NR.NP were less than in controls by 53% (p=0.008), 35% (p=0.01), and 65% (p=0.01), in *Flt23k*.NR.NP, Blank.NR.NP and sham groups, respectively (Fig. 3A). The volumes of fibrosis after RGD.*Flt23k*.NR.NP(n=14) treatment were less than in controls by 53% (n=16, p=0.002), 60% (n=8, p=0.005) and 60% (n=19, p=0.0003) in *Flt23k*.NR.NP, Blank.NR.NP and sham groups respectively (Fig. 3A).

In addition to suppressing CNV and fibrosis volumes in monkey, RGD.*Flt23k*.NR.NP appeared to substantially reduce the overall volumes of CNV in both the laser-induced and the AAV.shRNA.sFlt-1 murine models. In mouse laser-induced CNV, the overall volumes of CNV lesions regressed by 24% (n=11, p<0.05) at 2 weeks post-intervention in RGD.*Flt23k*.NR.NP, whereas *Flt23k*.NR.NP, RGD.Blank.NR.NP, Blank.NR.NP and sham

controls showed 12%, 8% reduction, 4% increase and 1% reductions in volume, respectively (Fig. 3B).There were no statistically significant differences observed among the control groups in both monkey and mouse laser induced CNV models. In the *sFlt-1* knockdown CNV murine model, the overall volumes of the classic CNV lesions at the injection site decreased by 43% (n=9) in RGD.*Flt23k*.NR.NP treated groups. By contrast, CNV lesion volumes increased by 3% (n=10, *p*=0.007), 33% (n=10, *p*=0.002), 54% (n=10, *p*=0.007), respectively in *Flt23k*.NR.NP, Blank.NR.NP, and sham controls at 4 weeks after treatment (Fig. 3C, D).Furthermore, the average fibrosis volume in the RGD.*Flt23k*.NR.NP group (n=10) was less than that of lesions in the *Flt23k*.NR.NP group by 43.9% (n=13; p=0.006) and by 51.8% *vs.* the Blank.NR.NP group (n=9; p=0.04). There was a non-significant difference (34.7%) *vs.* lesions in the RGD.NR.NP group (n=11; p=0.12) (Fig. S3). These results suggest that both angiogenesis and fibrosis are regressed by RGD.*Flt23k*.NR.NP treatment in established CNV, although RGD alone may be effective in ameliorating fibrosis. Furthermore, we observed even more striking results in the AAV.shRNA.sFlt-1 knockdown CNV murine model. Secondary CNV lesions developed in the controls but not in the mice treated with RGD.*Flt23k*.NR.NP (Fig. 3E), indicating RGD.*Flt23k*.NR.NP treatment might inhibit as well as regress CNV. We further compared the efficacy on CNV regression within travitreal injection of anti-mouse VEGF antibodies (comparable to clinically used antibody delivery in humans). RGD.*Flt23k*.NR.NP achieved a 24% reduction, which was greater than that achieved with antibody treatment (n=10, 2 weeks, p<0.05, Fig. 3F).

Vision function is restored exclusively after treatment with RGD.*Flt23k*.NR.NP

As laser-induced CNV models have a limited potential for recovery of visual function due to partial retinal burnout, an AAV.shRNA.*sFlt-1*-induced murine CNV model was used to test visual acuity and the treatments were repeated at 2 weeks post intervention. Whole-head optokinetic tracking (OKT) measurements were performed in a masked manner before treatment and at 2, 4 and 6 weeks post-treatment. All groups of *sFlt-1* knockdown-induced CNV exhibited comparable pre-treatment baseline levels of visual acuity (VA) whereas a significant VA increase of 9.4% was observed following RGD.*Flt23k*.NR.NP treatment (n=11, *p*= 0.03, Fig. 3G). Gradual yet progressive improvement in behavioral acuity was observed, from ~5% increase at 2 weeks post treatment to ~10% at 4 weeks. At 6 weeks, 85.7% of eyes in the treatment group showed improved VA greater than 10%. In contrast, no significant differences in VA were detected among the *Flt23k*.NR.NP, Blank.NR.NP, and vehicle treated control groups, suggesting that RGD.*Flt23k*.NR.NP nanoparticles effectively restored vision compromised by CNV.

No ocular or systemic toxicity was detected

Quantification of Nile Red levels in monkeys' serum (at day 1,7, 14 and day 30 post intravenous administration) indicated its concentrations were below quantification limit (BQL, 0.05 μM,) in all samples at all time points (Fig. S4), suggesting that amounts of nanoparticles remaining in the bloodstream 1 day after systemic administration were negligible. Nile Red levels were also assessed from the other collected monkey tissues (kidney, lung, skin, and liver) to estimate the percentage of nanoparticles which remained at day 30 post intervention. In all tissues, the levels of Nile Red were below quantifiable levels, although Nile red could be observed within CNV lesions in the RGD.*Flt23k*.NR.NP group by confocal microscopy (Fig. 2C), indicating that NP's were completely eliminated from systemic organs/tissues by 30 days post-administration.

Further, there was no ocular toxicity observed *in vivo* in any of the study animals. Examinations of animal eyes *in vivo* by experienced ophthalmologists using the Heidelberg Spectralis fundus imager revealed no ocular hemorrhage or inflammation, retinal

detachment, retinal degeneration or any other abnormalities indicating ocular toxicity. No significant retina morphological abnormalities via histological analysis of H&E staining were observed. Further, no retinal apoptosis (assessed by TUNEL staining) was detected in the retina outside the area of CNV lesions in any group at day 30 post-injection (Fig. 3 and Fig. 4A and B).

A masked experienced pathologist (LLE) performed microscopic examinations of monkey organ tissue sections. The liver, lung, kidney, and skin sections showed no significant histopathological changes at 1 month following intravenous delivery of nanoparticles (Fig. 4C). No abnormal health problems or other adverse events were reported in any monkeys within 30 days of treatment.

Discussion

In this study, we tested a novel delivery system with nonviral sustained-release gene therapy to treat rodent and primate models of CNV *in vivo*. We demonstrated that RGD targeting significantly enhances nanoparticles localization and concentration in CNV lesions, and that gene delivery of RGD-conjugated nanoparticles delivering plasmids expressing *Flt23k*, but not controls, via a single intravenous administration is efficacious in suppressing CNV and fibrosis. Furthermore, in a model of progressive CNV induced by knockdown of endogenous *sFlt-1*, CNV progression was inhibited and vision function was significantly restored after treatment. We observed no systemic or ocular toxicity after nanoparticle administration. Moreover, the data support the conclusion that the *Flt23k* component inhibits neovascularization while the RGD component also suppresses fibrosis, consistent with earlier reports of the activity of this peptide moiety.[26,32,33]

The recombinant gene is driven by a pCMV vector, which is not integrative; we previously confirmed the release of nanoparticles and the expression of Flt23K in the murine cornea by western blot *in vivo*.[28,34] Nanoparticles expressing the Flt23k recombinant peptide could last for 5–6 weeks after delivery.[28,34] The plasmid works to express Flt23k for 7–10 days in its naked form, and successfully block angiogenesis *in vitro* and *in vivo*.[17,35] In this study, nanoparticles expressing Flt23K after systemic delivery were observed for at least one month in primate eyes with CNV (Fig. 2C). However, they are not present in normal eyes or tissues 1 week after delivery (Fig. 2B). These characteristics are significant as they have the potential to improve anti-VEGF efficiency, decrease treatment frequency, reduce untargeted tissue and systemic side effects, and improve delivery to target tissues.

These findings bear particular import in light of studies showing that long-term intravitreal non-targeted anti-VEGF suppression is associated with subretinal fibrosis, choriocapillaris abnormalities, and optic nerve or photoreceptor degeneration,[12,36–38] effects which may be mitigated or avoided by our targeted approach and use of RGD. Further, VEGF has been shown to be important for choriocapillaris, cone, and ganglion cell homeostasis; non-targeted VEGF suppression through genetic modification or intravitreal neutralization results in retinal dysfunction, structural damage, and photoreceptor toxicity in a variety of animal models.[39–44] By targeting anti-VEGF therapy to CNV lesions using RGD-conjugated nanoparticles, our strategy would be expected to minimize or avoid these drawbacks. A previous study showed that ranibizumab treatment regressed CNV by approximately about 26% in monkeys;[45] whereas about a 65% regression in monkey CNV lesion volumes was observed in our study. While these studies are not directly comparable, these observations are encouraging, as is our finding that RGD.*Flt23k*.NR.NP achieved significantly more reduction in CNV volume in mice than intravitreal anti-mouse VEGF antibody injection. Furthermore, as the normal baseline level for C57Bl/6 mice is approximately 0.37 cycles/degree,[46] the 9.4% improvement (from 0.304 ± 0.009 to 0.331 ± 0.012 cycles/degree) after

targeted RGD.*Flt23k*nanoparticletreatment represents a restoration of approximately 40% of the visual acuity loss due to CNV. Approximately 86% of mice (6 of 7) showed an average improvement of vision by 12.2 ± 5.2 %. In 4 eyes (out of 14) there was an improvement of over 20% and acuity reached 0.371±0.013 cycles/degree after treatment (baseline acuity in normal mice).This would compare favorably with respect to AMD treatment in humans, where only one third of patients show overall gain of three lines in visual acuity with intravitreal anti-VEGF injection therapy.[10,12,29]

In this study, we used Flt23k nanoparticles as a stand-alone therapy to determine whether they could take the place of intravitreal anti-VEGF injections, which are used as first-line therapy for choroidal neovascularization. In earlier work,[50] we have previously used Flt23k nanoparticles in combination with triamcinolone for penetrating keratoplasty (corneal transplant), as triamcinolone is standard of care therapy in corneal transplant, and in that study, we sought to determine whether we could improve transplant success with using our anti-angiogenic nanoparticles. We found that the combination of steroids and Flt23k nanoparticles suppressed lymphangiogenesis and hemangiogenesis, synergistically improving transplant survival. Future studies for choroidal neovascularization should explore combination therapies with existing anti-VEGF regimens to see whether the frequency or cumulative dose of intravitreal injections can be reduced.

Although no ocular or systemic toxicity was observed in this study, defects in the eye, kidney, lung, heart, brain, or lungs may be detected after chronic exposure (repeated injections over an extended period of time). Therefore, further studies would be necessary before concluding this delivery system is completely safe.

In conclusion, RGD-targeted nanoparticles delivering *Flt23k*intraceptorplasmidsoffer a new pathway to ocular drug delivery via systemic administration, successfully suppressing neovascularization and fibrosis in models of macular degeneration while avoiding significant drawbacks associated with intraocular injection of anti-VEGF agents.

Methods

Preparation of anti-VEGF intraceptor plasmid-loaded PLGA nanoparticles

PLGA (Poly (lactide-co-glycolide)) Resomer 503H (50:50; i.v. 0.32–0.44 dl/g; Boehringer Ingelheim Chemicals, Petersburg, VA), Nile Red (Sigma Aldrich, St Louis, MO), and *Flt23k* plasmids were used in the preparation of *Flt23k*.NR nanoparticles. PLGA Resomer 503H (100mg) was dissolved in 1.75 ml of dichloromethane and Nile Red solution (250µl of a 1mg/ml solution in dichloromethane) was added to make up the volume to 2 ml. *Flt23k* plasmid (4mg) was suspended in TE buffer (500 µl).

The plasmid solution was emulsified with the PLGA solution in dichloromethane containing Nile Red by sonication with a probe sonicator (MisonixSonicator 3000) at 10W for 1 minute to form the primary emulsion. The primary emulsion was transferred to 10 ml of 2% aqueous polyvinyl alcohol (PVA) solution under sonication at 30W for 3 minutes to form the secondary emulsion. The secondary emulsion was kept stirring at room temperature for 4 hours. The suspension was further evaporated using a rotovap (Buchi Rotavapor R200; Buchi Analytical, New Castle, DE) for 2 hours at 37°C in a heated water bath (Buchi Heat Bath B490) to remove residual solvent. Following evaporation, nanoparticles were harvested by centrifugation at ~30000 g for 15 minutes at 4°C. The supernatant was discarded and the pellet of nanoparticles was re-dispersed in 25 ml of distilled water. The nanoparticles were recentrifuged at ~30000g for 15 minutes at 4°C. Two such washing steps were performed using distilled water to remove any surface bound PVA and plasmid. The final nanoparticle pellet was re-dispersed in 10 ml of distilled water and frozen at −80°C. The frozen

dispersion was then subjected to lyophilization (Labconcolyophilizer, Labconco Corporation, Kansas city, MO).

To prepare Nile Red loaded blank particles (Blank.NR.NP), the plasmid was excluded from the procedure described above and TE buffer (without plasmid) was added to form the primary emulsion. Drug content and particle size were characterized for the nanoparticles after lyophilization. Drug content was estimated using UV spectrophotometry, and particle size was measured using Malvern Nanosizer (Malvern Instruments, Ltd., Malvern, UK).

To prepare RGD.*Flt23k*.NR nanoparticles, conjugation of the RGD peptide was performed as follows. Plasmid-containing Nile Red-loaded nanoparticles (100mg, *Flt23k*.NR.NP) were weighed and dispersed in 15ml of 50mM MOPS buffer (Sigma Aldrich, St Louis, MO) by vortexing thoroughly for 15 minutes. The surface COOH groups were activated by incubation with EDAC (0.01 M, Ethyl-3-(3-dimethylaminopropyl) carbodiimide HCl (Sigma Aldrich, St Louis, MO) at room temperature for 2 hours with vortexing. A 10mM solution of RGD peptide (custom-synthesized by Genscript, Piscataway, NJ) in MOPS buffer (pH 6.5) was added dropwise to activated nanoparticles and vortexed at room temperature for 12 hours. Conjugated nanoparticles were separated by centrifugation ~30000 g for 15 minutes at 4°C and were lyophilized. The pellet was re-suspended in water and lyophilized as described previously.

Nanoparticle characterization

RGD.*Flt23k*.NR.NP, *Flt23k*.NR.NP, and Blank.NR.NP nanoparticles were characterized for plasmid content, particle size and polydispersity, and zeta potential.

Plasmid content determination: Plasmid loading in RGD.*Flt23k*.NR.NP and *Flt23k*.NR.NP nanoparticles was determined by dissolving 2mg of the nanoparticles in 1ml of dichloromethane and extracting the DNA into 1ml of water. The absorbance of the aqueous layer was measured at 260 nm using a UV spectrometer (Spectramax 250 microplate reader, Molecular Devices LLC, Sunnyvale, CA). Particle size and zeta potential measurement: One mg/ml nanoparticle dispersion was prepared in phosphate buffer saline (PBS pH 7.4). This dispersion was subjected to particle size and zeta potential measurement using Malvern Nanosizer (Malvern Instruments Ltd., Malvern, UK).

Preparation of nanoparticles suspension for intravenous delivery

Preparation of nanoparticles suspension for intravenous delivery is described in supplementary materials.

Animals

C57BL/6J mice aged 8–12 weeks[46] purchased from The Jackson Laboratory (The Jackson Laboratory, Bar Harbor, ME) were used for our experiments. Cynomolgus macaque monkeys (3 years of age; male or female, approximately 2.5 kg in weight) were purchased from PreLabs (Oak Park, IL). Experimental groups were age and sex matched. An intravenous scatheter was placed in the saphenous vein in the monkeys and routed to a subcutaneous access port for anesthesia and fluorescein administration during the study. The monkeys were fasted overnight prior to treatment and sedated for laser treatment and imaging with ketamine hydrochloride (10–20 mg/kg), atropine sulfate (0.02–0.04 mg/kg), and acepromazine maleate (0.05–0.1 mg/kg) to effect anesthesia. All the mice and monkeys were handled in accordance with the Association for Research in Vision and Ophthalmology (ARVO) Statement for the Use of Animals in Ophthalmic and Vision Research. Experiments were approved by the Institutional Animal Care and Use Committees (IACUCs) of the University of Utah and the University of Kentucky.

sFlt-1 knockdown-induced CNV models

sFlt-1 knockdown-induced CNV models were prepared as described previously.[30] Briefly, small hairpin ribonucleic acid (shRNA) expression cassettes (SECs) were developed by *in vitro* amplification using PCR. SECs are PCR products that consist of promoter and terminator sequences flanking a hairpin small interfering ribonucleic acid (siRNA) template. Multiple target sequences along with different combinations of promoters were screened to find the most effective siRNA capable of gene knockdown *in vitro* and *in vivo*. The best targets for soluble fms-like tyrosine kinase-1 (sFlt-1) (AAUGAUUGUACCACACAAAGU) were ligated into the pSEC Neo vector using EcoRI and HindIII (New England Biolabs, Beverly, MA). Plasmids were prepared (Plasmid Mini Prep kit, Eppendorf, New York City, NY) and sequenced to confirm the in-frame sequence of the inserts. From this plasmid, we developed shRNA.*sFlt-1* and shRNA.Negative cDNA with an H1 promoter. We used pAAV-MCS as a plasmid containing inverted terminal repeat _ENREF_2726, (AAV helper system, Agilent Technologies Inc, Santa Clara, USA). shRNA.*Flt-1* and sh.Negative cDNA with H1 promoter were inserted to pAAV using PstI site to generate pAAV.shRNA.*Flt-1* and pAAV.shRNA.Negative. To produce adeno-associated virus (AAV) vector (serotype2), we submitted both plasmids to the Viral Vector Core at the University of Massachusetts.

Mice were placed under general anesthesia with an intraperitoneal injection of tribromoethanol (Avertin®) (289mg /kg). Topical 0.5% proparacaine solution and 1% tropicamide ophthalmic solution were applied to the cornea to achieve topical anesthesia and mydriasis, respectively. Using an Olympus stereomicroscope for magnification, a small incision was made behind the limbus with a 30.5 gauge needle. To deliver AAV.shRNA.*sFlt-1* subretinally, a custom 33-gauge blunt tipped microsyringe (Hamilton Co., Reno, NV) was inserted through the incision and advanced gently across the vitreous behind the lens until it made contact with the neural retina. Gentle pressure was applied to the neural retina puncturing it to enter the subretinal space in the posterior pole. With the needle in position, the AAV vector carrying shRNA.*sFlt-1* was injected into the subretinal space creating a bleb. Dilated fundus examinations during the procedure showed partial retinal detachment seen as a bleb, confirming successful subretinal delivery. The mice were placed on a water circulating heat pad until recovery post-procedure and an antibiotic ointment was applied to the eye.

Laser-induced CNV murine and primate models

Laser-induced CNV murine and primate models were performed as described in the supplementary materials.

In vivo monitoring of nanoparticles and development of CNV

In vivo imaging of the retinal fundus was performed by Heidelberg Retina Angiography (HRA) and Optical Coherence Tomography (OCT) (Spectralis®, Heidelberg Engineering, Vista, CA) using the fluorescein angiograph (FA) and infrared (IR) modes separately. Three-dimensional scanning laser ophthalmoscope (SLO) images of the fundus were obtained using volume scans in the FA mode along with cross-sectional OCT images. SLO images were acquired using the FA mode to visualize the Nile Red loaded nanoparticles after intravenous injection.

Animals were anesthetized and pupils were dilated as described above. Mice were given intraperitoneal injections (0.1ml) or monkeys were given intravenous injections (0.1 ml/kg) of 10% Sodium fluorescein (Akorn, Inc, Lake Forest, IL) to acquire the FA images. Intravenous administrations of treatment and controls were performed immediately after imaging. Imaging was repeated and recorded by FA+OCT at 2 weeks or 4 weeks after intervention.

Computer-Assisted Quantitative Analysis of OCT Images

Quantification of lesions was performed in a similar approach to previously described techniques for calculating volumes of CNV in humans and retinal blastomas in mouse models.[30,47–49] B-scans were exported from Heidelberg Eye Explorer (HEE), Heidelberg's image analysis software, in .jpeg format and imported as complete stacks into Seg3D software. Seg3D is a segmentation processing and analyzing tool developed by the University of Utah Scientific Computing and Imaging Institute and the NIH/NCRR Center for Integrative Biomedical Computing (Volumetric Image Segmentation and Visualization. Scientific Computing and Imaging Institute, available: http://www.seg3d.org).Boundaries of the CNV lesion and deformations of the RPE were manually outlined using a polyline tool by 2 graders in a masked manner (TM, KJ). Seg3D masked the region enclosed within the polyline for each consecutive b-scan in pixels squared. An automated feature of Seg3D calculated two-dimensional lesion area, summing the masked b-scans for each stack. Scaling factors obtained from HEE were used to convertpixel^2 to μm^2. After adjusting the corneal curvature to 1.4mm[48], the scaling factors for the x and z-axes were 1.45 ± 2 and 3.87 μm/ pixel respectively. To calculate lesion volume (μm^3) the spacing between each line scan, the area was multiplied by the distance (52 ± 2 μm) between scans between scans also provided by HEE software. Finally, estimated volumes were converted to mm^3 and reported.

To quantify the CNV or fibrosis membrane volume using immunostained choroidal flat mounts, horizontal optical sections (3.87µm/step) were obtained starting from the surface of the RPE-choroid-sclera complex to the deepest focal plane of the choroidal neovascular tuft. Images of each section were stored digitally. CNV or fibrosis was identified by setting a threshold level of fluorescence above which only vessels were captured. The area of CNV or fibrosis-related fluorescence was measured by image analysis software accompanying the microscope. The sum of the entire area of fluorescence in each horizontal section was used as an index of the volume of CNV or fibrosis membrane. Images of each section were stored digitally. The volumes were measured by image analysis software.

Cryosections and flat mounts

Cryosections and flat mounts were prepared as described in the supplementary materials.

Immunostaining

To stain CNV or fibrosis,*Griffonia simplicifolia* Alexa Fluor® 546conjugated isolectin (1:200, Life Technologies Corporation, Carlsbad, CA), rat anti-heparan sulfate proteoglycan (Perlecan) monoclonal antibody (1:200,clone A7L6, EMD Millipore Corporation, Billerica, MA), and rabbit polyclonal anti-Collagen I (1:40, Abcam Inc., Cambridge, MA) were used as primary antibodies. Alexa Fluor488 goat anti rabbit (1:400, Life Technologies Corporation, Carlsbad, CA) and FITC secondary antibody (1:1000, Anti-Rat IgG-FITC, F6258, Sigma-Aldrich, St. Louis, MO) were used as secondary antibodies. To stain alpha5, rabbit anti-Integrin alpha5 (1:200, EMD Millipore Corporation, Billerica, MA) was used as primary antibody and Alexa Fluor546 goat anti-rabbit (1:200, Life Technologies Corporation, Carlsbad, CA) was used as secondary antibody.

Cryosections were baked at 37°C for 40 minutes. Following this, they were washed three times with PBS and then incubated in 10% goat serum (Abcam Inc., Cambridge, MA) diluted in IHC buffer (1% BSA, 1% FBS, and 0.3% Triton X-100 in PBS [pH 7.4]) for 1 hour. They were then incubated with primary antibodies overnight at 4°C. After primary antibody incubation, slides were washed and incubated in secondary antibodies for 1 hour at room temperature (RT). They were then washed 3 times with PBS, after which VECTASHIELD® Mounting Medium with DAPI (Vector Laboratories Inc., Burlingame, CA) was applied and cover slips were placed on the slides. After incubation with secondary

antibody in monkey sections, 0.3% Sudan Black (w/v) (Sigma Aldrich, St. Louis, MO, USA) in 70% EtOH (v/v) was applied to slides for 10 minutes in order to quench the autofluorescence. Slides were then rinsed quickly with PBS 8 times and mounted as above.

To stain murine and monkey flat mount sections, sections were washed twice with PBS for 30 minutes at 4°C with shaking. They were then incubated successively in 50%, 75%, and 100% methanol for 30 minutes each to dehydrate the tissue. This was followed by successive incubation in 100%, 75%, 50%, and 25% methanol at room temperature for 30 minutes each to rehydrate the sample. They were then washed 2 times in PBS for 30 minutes 4°C, followed by incubation in blocking buffer (1% BSA /0.5 % Triton-X /PBS) for 60 minutes at RT. Primary antibodies were incubated overnight at 4°C as above. Samples were then washed with 0.1 % Triton-X/PBS 3 times for 30 minutes at 4°C. As described above, secondary antibodies were then incubated for 2 hours at RT, followed by washing with PBS 2 times for 30 minutes at 4°C. 0.3% Sudan Black was then used as above to quench the autofluorescence.

H&E Staining

Samples were sectioned at 1 μm or 3 μm for hematoxylin and eosin (H&E) staining (described in supplementary materials). All fluorescent sections and H&E stained sections were imaged with an Axiovert 200 microscope (Carl Zeiss Micro Imaging, Inc., Thornwood, NY) equipped with confocal epifluorescence illumination or an Axion Cam MR digital camera (Carl Zeiss Micro Imaging, Inc., Thornwood, NY) and processed using Adobe® Photoshop® software (Adobe Systems Incorporated, San Jose, CA). Unstained tissue sections were mounted and cover slipped and then directly examined under the above microscopes.

Nile Red quantification in Serum/Plasma and Organ/Tissues

Nile Red was quantified using dichloromethane (DCM) by liquid-liquid extraction method as described below: Serum: 0.2 mL of the study sample was transferred to a polypropylene tube and 2.0 mL of DCM was added. All tubes were vortexed for 30 seconds and centrifuged using Eppendorf centrifuge at 12,000 rpm for 8 min. Organ/tissues: All the collected tissues were weighed and transferred to clean glass tubes; 2.0 mL of DCM was added and homogenized using homogenizer (Polytron 3100D, Kinematica, Inc., Bohemia, NY) at 10,000 rpm for 5 min, to disrupt the tissue and to get a homogeneous suspension. The obtained suspensions were transferred to 2 mL polypropylene tubes after vortexing for 30 seconds. Tubes were centrifuged at 12,000 rpm for 8 min.

The supernatant was collected from all samples and Nile Red fluorescence was measured by a custom-built fluorometer. The excitation light from a green LED was filtered through 540+20 nm interference filter. The emission was collected through a long pass filter at 630 nm and detected by a photomultiplier tube (H5783, Hamamatsu Corp., Bridgewater, NJ). All the study samples were read against a standard calibration curve constructed using known quantities of Nile Red. The curve was linear between 0.05 and 1.0 μM (Fig.S4).

Testing visual performance

We tested mouse vision using their optomotor reflex, an involuntary head turning in response to the movement of a vertical sinusoidal grating pattern. We used the OptoMotry System (Cerebral Mechanics, Lethbridge, AB, Canada) to display a virtual rotating cylinder of sinusoidal grating created by 4 liquid crystal displays, one on each side of the box. A mouse was placed on a pedestal inside this box with a fixed video camera looking down at it from the top. The video acquisition displayed on the monitor was used to follow and classify mouse movements (tracking *vs.* non-tracking). Spatial frequency of the stimulus was

changed between 0.042 cycles/degree and 0.700 cycles/degree, whereas rotation speed (12 degrees/s) and contrast (100%) were kept constant. Spatial frequency of the stimulus was stepped up or down with the staircase method to find the behavioral threshold, corresponding to the visual acuity for the behavior. Tracking was defined as a smooth pursuit movement concordant with the velocity and direction of the stimulus. Trials of each direction and spatial frequency were repeated until the presence or absence of the tracking response could be established unequivocally. Measurements were conducted in masked fashion, *i.e.*, the operator did not know which experimental group the measured mice belonged to.

TUNEL Assay

Enucleated eyes were fixed in 4% PFA/PBS for 2 hours at 4°C, followed by cryoprotection in 15% sucrose/PBS 1 hour then changed to 30% sucrose/PBS overnight at 4°C. 12 μm embedded frozen sections were further processed for TUNEL staining using Click-iT® TUNEL Alexa Fluor® image assay kit (Cat. No. C10246, Life Technologies, Carlsbad, CA) according to the manufacturer's instructions. A positive control was set up by treatment with DNase I. Retina sections were furthered counterstained with Hoechst 33342 to identify the retinal cell layers. Inverted Fluorescence microscope (Carl Zeiss Micro Imaging, Inc., Thornwood, NY) was used to capture images.

Statistical analysis

Differences in CNV volumes were compared with the Mann Whitney U test with Bonferroni correction for multiple comparisons. Correlation analysis was performed using Pearson's correlation. Two-tailed paired T-test was used to test optometry in the comparison of before treatment versus after treatment data. *P* values < 0.05 were considered significant. Data are presented as mean ± s.e.m.

Supplementary Material

Refer to Web version on PubMed Central for supplementary material.

Acknowledgments

References

1. Ambati J, Ambati BK, Yoo SH, Ianchulev S, Adamis AP. Age-Related Macular Degeneration: Etiology, Pathogenesis, and Therapeutic Strategies. Surv Ophthalmol. 2003:257–293. [PubMed: 12745003]

2. Bunce C, Xing W, Wormald R. Causes of Blind and Partial Sight Certifications in England and Wales: April 2007–March 2008. Eye (Lond). 2010:1692–1699. [PubMed: 20847749]

3. Jager RD, Mieler WF, Miller JW. Age-Related Macular Degeneration. N Engl J Med. 2008:2606–2617. [PubMed: 18550876]

4. Pascolini D, Mariotti SP, Pokharel GP, Pararajasegaram R, Etya'ale D, Negrel AD, Resnikoff S. 2002 Global Update of Available Data on Visual Impairment: A Compilation of Population-Based Prevalence Studies. Ophthalmic Epidemiol. 2004:67–115. [PubMed: 15255026]

5. Alon T, Hemo I, Itin A, Pe'er J, Stone J, Keshet E. Vascular Endothelial Growth Factor Acts as a Survival Factor for Newly Formed Retinal Vessels and Has Implications for Retinopathy of Prematurity. Nat Med. 1995:1024–1028. [PubMed: 7489357]

6. Carmeliet P, Jain RK. Molecular Mechanisms and Clinical Applications of Angiogenesis. Nature. 2011:298–307. [PubMed: 21593862]

7. Ferrara N, Davis-Smyth T. The Biology of Vascular Endothelial Growth Factor. Endocr Rev. 1997:4–25. [PubMed: 9034784]

8. Ferrara N, Gerber HP. The Role of Vascular Endothelial Growth Factor in Angiogenesis. Acta Haematol. 2001:148–156. [PubMed: 11815711]

9. Gragoudas ES, Adamis AP, Cunningham ET Jr. Feinsod M, Guyer DR. Pegaptanib for Neovascular Age-Related Macular Degeneration. N Engl J Med. 2004:2805–2816. [PubMed: 15625332]

10. Brown DM, Kaiser PK, Michels M, Soubrane G, Heier JS, Kim RY, Sy JP, Schneider S. Ranibizumab Versus Verteporfin for Neovascular Age-Related Macular Degeneration. N Engl J Med. 2006:1432–1444. [PubMed: 17021319]

11. Rosenfeld PJ, Brown DM, Heier JS, Boyer DS, Kaiser PK, Chung CY, Kim RY. Ranibizumab for Neovascular Age-Related Macular Degeneration. N Engl J Med. 2006:1419–1431. [PubMed: 17021318]

12. Bhisitkul, R. 2011 UCSF Ophthalmology Update (Dec. 2–3, 2011). SAn Francisco, CA: 2011. 7 Year Update on the Anchor/Marina Ranibizumab Cohort :The Seven up Study.

13. Jackson TL, Kirkpatrick L. Cost Comparison of Ranibizumab and Bevacizumab. BMJ. 2011:d5058. [PubMed: 21862536]

14. Singh SR, Grossniklaus HE, Kang SJ, Edelhauser HF, Ambati BK, Kompella UB. Intravenous Transferrin, Rgd Peptide and Dual-Targeted Nanoparticles Enhance Anti-Vegf Intraceptor Gene Delivery to Laser-Induced Cnv. Gene Ther. 2009:645–659. [PubMed: 19194480]

15. Jani PD, Singh N, Jenkins C, Raghava S, Mo Y, Amin S, Kompella UB, Ambati BK. Nanoparticles Sustain Expression of Flt Intraceptors in the Cornea and Inhibit Injury-Induced Corneal Angiogenesis. Invest Ophthalmol Vis Sci. 2007:2030–2036. [PubMed: 17460257]

16. Hsieh WJ, Liang CJ, Chieh JJ, Wang SH, Lai IR, Chen JH, Chang FH, Tseng WK, Yang SY, Wu CC, et al. In Vivo Tumor Targeting and Imaging with Anti-Vascular Endothelial Growth Factor Antibody-Conjugated Dextran-Coated Iron Oxide Nanoparticles. Int J Nanomedicine. 2012:2833–2842. [PubMed: 22745546]

17. Singh N, Amin S, Richter E, Rashid S, Scoglietti V, Jani PD, Wang J, Kaur R, Ambati J, Dong Z, et al. Flt-1 Intraceptors Inhibit Hypoxia-Induced Vegf Expression in Vitro and Corneal Neovascularization in Vivo. Invest Ophthalmol Vis Sci. 2005:1647–1652. [PubMed: 15851564]

18. Halbert CL, Miller AD, McNamara S, Emerson J, Gibson RL, Ramsey B, Aitken ML. Prevalence of Neutralizing Antibodies against Adeno-Associated Virus (Aav) Types 2, 5, and 6 in Cystic Fibrosis and Normal Populations: Implications for Gene Therapy Using Aav Vectors. Hum Gene Ther. 2006:440–447. [PubMed: 16610931]

19. Thomas CE, Ehrhardt A, Kay MA. Progress and Problems with the Use of Viral Vectors for Gene Therapy. Nat Rev Genet. 2003:346–358. [PubMed: 12728277]

20. Tweden KS, Harasaki H, Jones M, Blevitt JM, Craig WS, Pierschbacher M, Helmus MN. Accelerated Healing of Cardiovascular Textiles Promoted by an Rgd Peptide. J Heart Valve Dis. 1995:S90–97. [PubMed: 8581220]

21. Zahn G, Vossmeyer D, Stragies R, Wills M, Wong CG, Loffler KU, Adamis AP, Knolle J. Preclinical Evaluation of the Novel Small-Molecule Integrin Alpha5beta1 Inhibitor Jsm6427 in Monkey and Rabbit Models of Choroidal Neovascularization. Arch Ophthalmol. 2009:1329–1335. [PubMed: 19822850]

22. Santos SC, Dias S. Internal and External Autocrine Vegf/Kdr Loops Regulate Survival of Subsets of Acute Leukemia through Distinct Signaling Pathways. Blood. 2004:3883–3889. [PubMed: 14726393]

23. Nomura M, Yamagishi S, Harada S, Hayashi Y, Yamashima T, Yamashita J, Yamamoto H. Possible Participation of Autocrine and Paracrine Vascular Endothelial Growth Factors in Hypoxia-Induced Proliferation of Endothelial Cells and Pericytes. J Biol Chem. 1995:28316–28324. [PubMed: 7499331]

24. Rosenfeld PJ, Shapiro H, Tuomi L, Webster M, Elledge J, Blodi B. Characteristics of Patients Losing Vision after 2 Years of Monthly Dosing in the Phase Iii Ranibizumab Clinical Trials. Ophthalmology. 2011:523–530. [PubMed: 20920825]

25. Gailit J, Clarke C, Newman D, Tonnesen MG, Mosesson MW, Clark RA. Human Fibroblasts Bind Directly to Fibrinogen at Rgd Sites through Integrin Alpha(V)Beta3. Exp Cell Res. 1997:118–126. [PubMed: 9141628]

26. Kotoh K, Nakamuta M, Kohjima M, Fukushima M, Morizono S, Kobayashi N, Enjoji M, Nawata H. Arg-Gly-Asp (Rgd) Peptide Ameliorates Carbon Tetrachloride-Induced Liver Fibrosis Via Inhibition of Collagen Production and Acceleration of Collagenase Activity. Int J Mol Med. 2004:1049–1053. [PubMed: 15547672]

27. Qazi Y, Stagg B, Singh N, Singh S, Zhang X, Luo L, Simonis J, Kompella UB, Ambati BK. Nanoparticle-Mediated Delivery of Shrna.Vegf-a Plasmids Regresses Corneal Neovascularization. Invest Ophthalmol Vis Sci. 2012:2837–2844. [PubMed: 22467572]

28. Amrite AC, Kompella UB. Size-Dependent Disposition of Nanoparticles and Microparticles Following Subconjunctival Administration. J Pharm Pharmacol. 2005:1555–1563. [PubMed: 16354399]

29. Martin DF, Maguire MG, Fine SL, Ying GS, Jaffe GJ, Grunwald JE, Toth C, Redford M, Ferris FL 3rd. Ranibizumab and Bevacizumab for Treatment of Neovascular Age-Related Macular Degeneration: Two-Year Results. Ophthalmology. 2012:1388–1398. [PubMed: 22555112]

30. Lou L, Ambati BK. Photoreceptor Avascular Privilege Is Due to Soluble Vegf Receptor-1. Submitted to Nature Medicine. 2012

31. Vasir JK, Labhasetwar V. Quantification of the Force of Nanoparticle-Cell Membrane Interactions and Its Influence on Intracellular Trafficking of Nanoparticles. Biomaterials. 2008:4244–4252. [PubMed: 18692238]

32. Wang LS, Chen YW, Li DG, Lu HM. Arg-Gly-Asp-Mannose-6-Phosphate Inhibits Activation and Proliferation of Hepatic Stellate Cells in Vitro. World J Gastroenterol. 2006:1303–1307. [PubMed: 16534891]

33. Xu XD, Liang L, Chen CS, Lu B, Wang NL, Jiang FG, Zhang XZ, Zhuo RX. Peptide Hydrogel as an Intraocular Drug Delivery System for Inhibition of Postoperative Scarring Formation. ACS Appl Mater Interfaces. 2010:2663–2671. [PubMed: 20707334]

34. Amrite AC, Edelhauser HF, Singh SR, Kompella UB. Effect of Circulation on the Disposition and Ocular Tissue Distribution of 20 Nm Nanoparticles after Periocular Administration. Mol Vis. 2008:150–160. [PubMed: 18334929]

35. Singh N, Jani PD, Suthar T, Amin S, Ambati BK. Flt-1 Intraceptor Induces the Unfolded Protein Response, Apoptotic Factors, and Regression of Murine Injury-Induced Corneal Neovascularization. Invest Ophthalmol Vis Sci. 2006:4787–4793. [PubMed: 17065489]

36. Ahlers C, Golbaz I, Stock G, Fous A, Kolar S, Pruente C, Schmidt-Erfurth U. Time Course of Morphologic Effects on Different Retinal Compartments after Ranibizumab Therapy in Age-Related Macular Degeneration. Ophthalmology. 2008:e39–46. [PubMed: 18675694]

37. Bellerive C, Cinq-Mars B, Lalonde G, Malenfant M, Tourville E, Tardif Y, Giasson M, Hebert M. Bevacizumab and Ranibizumab for Neovascular Age-Related Macular Degeneration: A Treatment Approach Based on Individual Patient Needs. Can J Ophthalmol. 2012:165–169. [PubMed: 22560423]

38. Marneros AG, Fan J, Yokoyama Y, Gerber HP, Ferrara N, Crouch RK, Olsen BR. Vascular Endothelial Growth Factor Expression in the Retinal Pigment Epithelium Is Essential for Choriocapillaris Development and Visual Function. Am J Pathol. 2005:1451–1459. [PubMed: 16251428]

39. Kurihara T, Westenskow PD, Bravo S, Aguilar E, Friedlander M. Targeted Deletion of Vegfa in Adult Mice Induces Vision Loss. J Clin Invest. 2012:4213–4217. [PubMed: 23093773]

40. Murakami Y, Ikeda Y, Yonemitsu Y, Miyazaki M, Inoue M, Hasegawa M, Sueishi K, Ishibashi T. Inhibition of Choroidal Neovascularization Via Brief Subretinal Exposure to a Newly Developed Lentiviral Vector Pseudotyped with Sendai Viral Envelope Proteins. Hum Gene Ther. 2010:199–209. [PubMed: 19778186]

41. Nishijima K, Ng YS, Zhong L, Bradley J, Schubert W, Jo N, Akita J, Samuelsson SJ, Robinson GS, Adamis AP, et al. Vascular Endothelial Growth Factor-a Is a Survival Factor for Retinal Neurons and a Critical Neuroprotectant During the Adaptive Response to Ischemic Injury. Am J Pathol. 2007:53–67. [PubMed: 17591953]

42. Quaggin SE. Turning a Blind Eye to Anti-Vegf Toxicities. J Clin Invest. 2012:3849–3851. [PubMed: 23093785]

43. Saint-Geniez M, Maharaj AS, Walshe TE, Tucker BA, Sekiyama E, Kurihara T, Darland DC, Young MJ, D'Amore PA. Endogenous Vegf Is Required for Visual Function: Evidence for a Survival Role on Muller Cells and Photoreceptors. PLoS One. 2008:e3554. [PubMed: 18978936]

44. Takeda A, Baffi JZ, Kleinman ME, Cho WG, Nozaki M, Yamada K, Kaneko H, Albuquerque RJ, Dridi S, Saito K, et al. Ccr3 Is a Target for Age-Related Macular Degeneration Diagnosis and Therapy. Nature. 2009:225–230. [PubMed: 19525930]

45. Goody RJ, Hu W, Shafiee A, Struharik M, Bartels S, Lopez FJ, Lawrence MS. Optimization of Laser-Induced Choroidal Neovascularization in African Green Monkeys. Exp Eye Res. 2011:464–472. [PubMed: 21414311]

46. Redfern WS, Storey S, Tse K, Hussain Q, Maung KP, Valentin JP, Ahmed G, Bigley A, Heathcote D, McKay JS. Evaluation of a Convenient Method of Assessing Rodent Visual Function in Safety Pharmacology Studies: Effects of Sodium Iodate on Visual Acuity and Retinal Morphology in Albino and Pigmented Rats and Mice. J Pharmacol Toxicol Methods. 2011:102–114.

47. Furino C, Ferrara A, Cardascia N, Besozzi G, Alessio G, Sborgia L, Boscia F. Combined Cataract Extraction and Intravitreal Bevacizumab in Eyes with Choroidal Neovascularization Resulting from Age-Related Macular Degeneration. J Cataract Refract Surg. 2009:1518–1522. [PubMed: 19683147]

48. Ruggeri M, Tsechpenakis G, Jiao S, Jockovich ME, Cebulla C, Hernandez E, Murray TG, Puliafito CA. Retinal Tumor Imaging and Volume Quantification in Mouse Model Using Spectral-Domain Optical Coherence Tomography. Opt Express. 2009:4074–4083. [PubMed: 19259247]

49. Schmucker C, Schaeffel F. A Paraxial Schematic Eye Model for the Growing C57bl/6 Mouse. Vision Res. 2004:1857–1867. [PubMed: 15145680]
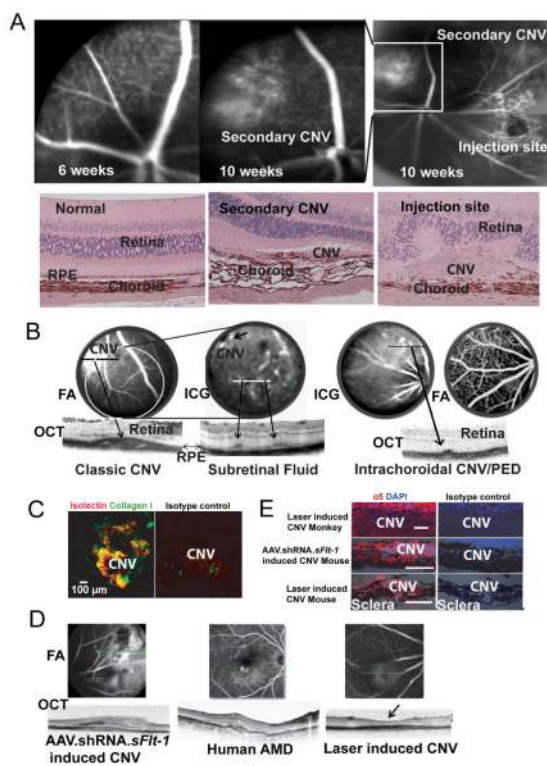
Fig. 1. Knockdown (AAV.shRNA.*sFlt-1*) induces murine CNV
(A) Secondary CNV was observed late and distant from injection site on fluorescein angiography (FA, top). Secondary CNV was detected at 10 weeks at a location where CNV was not observed by imaging at 6 weeks after injection and was distant from primary CNV at the injection site. H&E staining (bottom) shows the histology of normal retina, secondary CNV and classic CNV from the injection site in the *sFlt-1* knockdown mouse (6 months after injection), respectively (40×). **(B)** Classic CNV, subretinal fluid and intrachoroidal CNV or occult CNV were detected in the same eye (at 6 months).(PED: Pigment epithelial detachment; the top row images are Indocyanine Green (ICG)Angiography images.**(C)** IHC staining on choroidal flat mounts from *sFlt-1* knockdown eyes (6 months after injection) showed neovessels (isolectin) and fibrosis (collagen I) in CNV site. **(D)** The morphology of *sFlt-1* knockdown induced CNV closely mimics human CNV (from the database of Heidelberg Spectralis imager), while the retina in laser-induced CNV eyes displays partial burnout (arrow). **(E)** IHC staining demonstrates that alpha5 integrin was expressed strongly in all three types of CNV models (scale bar: 100 µm).
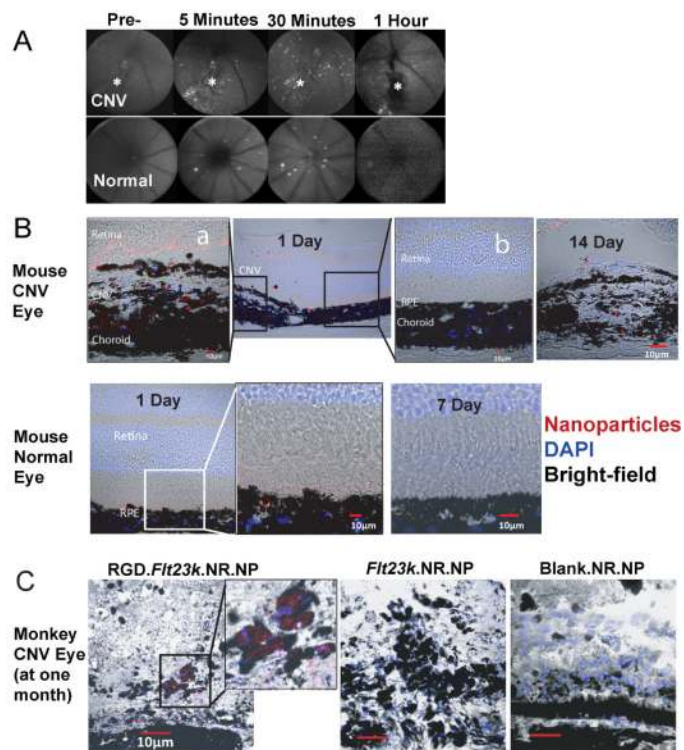
Fig. 2. RGD-functionalized nanoparticles localize to CNV lesions

(A) RGD.*Flt23k*.NR.NP was detected by the Spectralis imager *in vivo* in CNV eyes and normal eyes. **(B)** On histological confocal examination of murine ocular cryosections, more nanoparticles are present in eyes with CNV than in normal eyes. Nanoparticles were concentrated in CNV lesions at 24 hours post-intravenous injection. RGD-conjugated nanoparticles were detected in CNV lesions 14 days post-injection while only up to 7 days in normal eyes. **(a, b)** Magnified images from the frames show nanoparticles in CNV site and normal site in the same eye. **(C)** In laser-induced CNV monkey eyes one month post-intervention, some RGD-conjugated nanoparticles could still be detected in CNV lesion. However, unconjugated or blank nanoparticles were not found in CNV lesions.
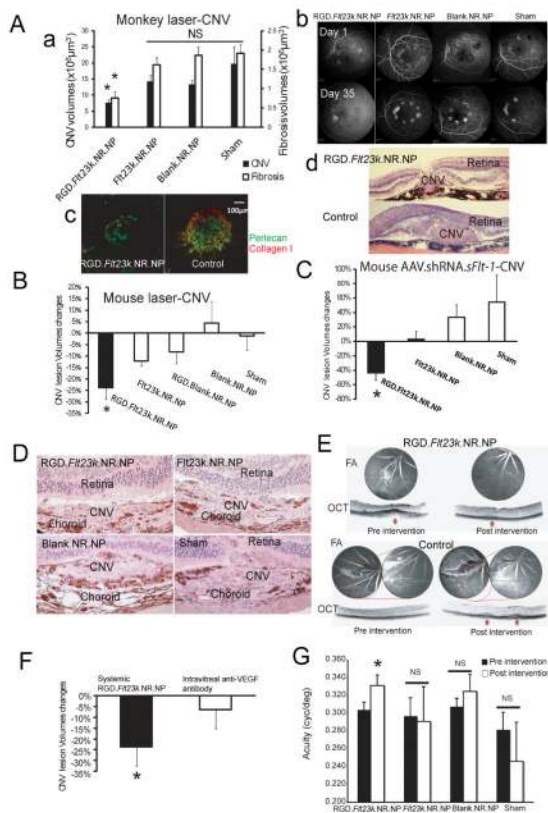
Fig. 3. Angiogenesis is inhibited in all CNV models, accompanied by restored vision in CNV eyes induced by *sFlt-1* knockdown

(A) In the laser-induced CNV monkey model, the volumes of CNV lesions, including neovessels (stained by perlecan) and fibrosis (stained by collagen I), significantly decreased 4 weeks after RGD.*Flt23k*.NR.NP treatment **(a)**. Representative images of FA **(b)**, IHC staining**(c)** and H&E staining **(d)**show the different size of CNV in each group. **(B)** In laser-induced CNV mice, CNV lesions were regressed byRGD.*Flt23k*.NR.NPtwo weeks post-intervention. **(C)** In the *sFlt-1* knockdowninduced murine CNV model, the volumes of CNV lesions were significantly decreased by RGD.*Flt23k*.NR.NP at 4 weeks after treatment. **(D)** Representative FA and OCT images detected the decreased CNV in treated mice from Fig. 3C, and detected increased CNV accompanied with secondary CNV occurrence in controls (arrows point to CNV). **(E)** Representative H&E images of each group in Fig. 3C show the different sizes of CNV after intervention. **(F)** Single systemic administration of RGD.*Flt23k*.NR.NP regressed CNV more than intravitreal anti-VEGF antibody. **(G)** Optomotor testingvision function was partially restored after 4 weeks treatment with RGD.*Flt23k*.NR.NP but not with the vehicle or sham controls.
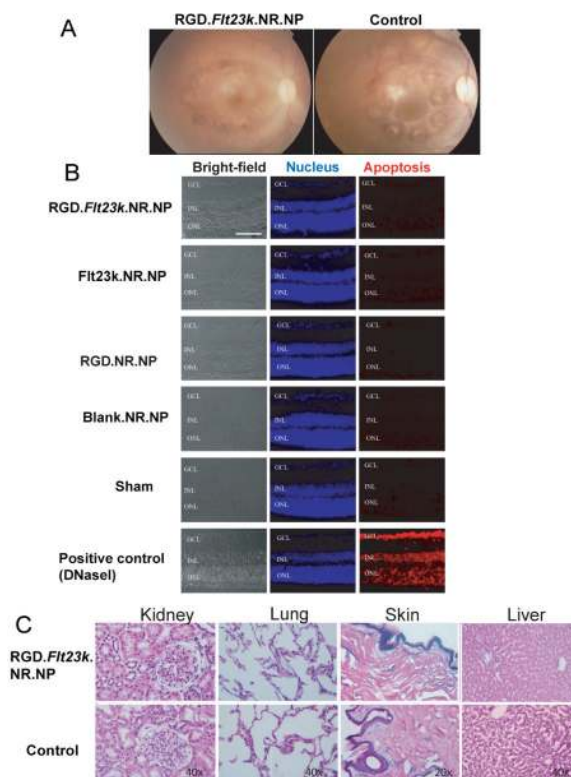
Fig. 4. Ocular and systemic toxicity were not detected after RGD.*Flt23k*.NR.NP treatment
Representative monkey ocular fundus images 30 days after intervention showed no
significant retinal morphological difference between treatment and control. **(B)** No apoptosis
in the retina outside the CNV lesions was detected at day 30 post intervention by TUNEL
staining (Scale bar: 100µm). **(C)** H&E images showed no significant histopathological
changes in the liver, lung, kidney, and skin sections after intravenous delivery of
nanoparticles in comparison to untreated, normal organs (30 days).

Table

Characterization of RGD.*Flt23k*.NR.NP, *Flt23k*.NR.NP, and Blank.NR.NP. Data is represented as mean ± S.D. (n=8).

Nanoparticle	Plasmid loading (% w/w)	Particle Size (nm ± S.D.)	Polydispersity index (± S.D.)	Zeta Potential (mV ± S.D.)
RGD.*Flt23k*.NR.NP	1.02	572.45 (± 37.43)	0.159 (± 0.027)	−2.11 ± 7.36
Flt23k.NR.NP	1.30	522.91 (± 12.59)	0.111 (± 0.044)	−22.67 ± 7.55
RGD.Blank.NR.NP	NA	163.7 (± 13.3 nm)	0.349 (±0.08)	−0.591 ± 0.04
Blank.NR.NP	NA	529.88 (± 29.01)	0.129 (± 0.031)	−27.69 ± 7.10